

Determination of Electron Energy Bands by Phase-Shift Parametrization: Application to Silver

Bernard R. Cooper and Elise L. Kreiger

General Electric Research and Development Center, Schenectady, New York 12301

and

Benjamin Segall

Department of Physics, Case Western Reserve University, Cleveland, Ohio 44106

(Received 4 March 1971)

We discuss a band parametrization scheme (within the framework of the Green's-function method, i. e., the Korringa-Kohn-Rostoker-type theory) specifying the phase shifts η_0 , η_1 , and η_2 as functions of energy. This approach is particularly useful for the noble and transition metals, where both d -band and free-electron-like effects are important. The $\eta_l(E)$ for a family of elements are expected to have characteristic energy dependences, with each $\eta_l(E)$ being specified over a substantial energy range by a few parameters. Such a parametrization scheme serves to present the information contained in an electron energy-band structure in a form in which one can conveniently blend empirical information with the results of first-principles calculations. First, we show the existence and form of the characteristic energy dependence of the $\tan\eta_l$'s for the noble metals. We then use our phase-shift parametrization scheme in a semiempirical way to find the band structure of Ag. To do this, we use a first-principles calculation as a guide, and adjust the parameters specifying the $\tan\eta_l$'s to fit some available Fermi-surface, optical, and photoemission data. The realistic phase shifts so obtained correspond to a modified crystal potential. Thus the semiempirical phase-shift parametrization scheme offers a practical and conceptually clear way of effectively incorporating experimental information about the solid state into the potential.

I. INTRODUCTION

In recent years there has been much interest in the development of parametrization and interpolation schemes for describing electron energy-band structures.¹⁻³ Broadly speaking, there are two related reasons for the development of such schemes. Clearly, for a given potential, current technique in first-principles band calculations allows one to calculate accurately the band structure and related physical quantities. Thus one aim of interpolation and parametrization schemes is to present the energy-band information in a form so flexible and simple as to be convenient for treating rather complex properties of solids in a realistic way. This is basically a matter of computational speed, i. e., making approximations that cast the theory into a form suitable for minimizing the time required in computations involving fast digital computers. Such speed may, for example, make self-consistent calculations feasible in a desired situation (say for studying magnetic properties of metals), or allow a very large number of points within the Brillouin zone to be treated, as is desirable when considering optical properties. A second aim of parametrization schemes is to blend empirical information with the results of first-principles calculations. Such a blending allows one to adjust the phase shifts obtained in *a priori* calculation so as to yield energy

bands consistent with experimental data. The realistic phase shifts so obtained correspond to a modified crystal potential. (Of course, in practice one often tries to satisfy these two interrelated aims at the same time.)

This separation between information describing the potential, and the calculation of the band structure once the potential is specified, is made particularly clear in the Green's-function formalism. There, for a muffin-tin potential, all the information about the potential is contained in the phase shifts or logarithmic derivatives of the radial wave functions; while the lattice-structure information is contained in the structure coefficients, the calculation of which takes the majority of computational time. With this in mind, we have developed an energy-band parametrization scheme⁴ within the framework of the Green's-function [Korringa-Kohn-Rostoker (KKR)] method.⁵ Our efforts have been devoted to the second of the two aims mentioned above, viz., effectively incorporating experimental information about the solid state into the potential or, strictly speaking, into the phase shifts for the electrons in the solid. Our emphasis has been on developing a scheme that is useful and accurate across the energy range (~ 1 Ry) necessary to treat the complete band structure for a typical metal. As an example of the use of such a scheme, we have developed a semiempirical band structure for silver.

Such a parametrization scheme is based on two facts. First is that in the KKR method the effects of the crystal potential are entirely embodied in the phase shifts $\eta_l(E)$ and are completely separated from crystal-structure effects. Second, because of the very rapid convergence of the Green's-function method, it suffices—except perhaps for very heavy metals—to include only the $l=0, 1,$ and 2 angular momentum components (and thus three phase shifts in a nonrelativistic calculation) in order to achieve high accuracy in the energy eigenvalues $E(\vec{k})$.

Our scheme is based on the expectation that the energy dependence of the phase shifts can be represented accurately over a wide range of energy with a limited number of parameters. Moreover, we expect that the parametric form for the energy dependence of the phase shifts will be the same for a family of elements. Once that form is established, one can obtain a particular band structure by simply adjusting the values of the parameters to agree with some first-principles calculational results and/or empirical data. In Sec. II, we have verified that the expectation is justified for the noble metals (for the present omitting relativistic considerations) by finding one parametric form (for each l value) for the $l=0, 1,$ and 2 phase shifts which allows one to fit the band structures obtained by first-principles calculation for two potentials each for Cu and Ag with high accuracy. Moreover, we show that with one simple, and rather obvious, alteration, the same parametric forms describe the band structure of Al. Thus the forms we find for the energy-dependent phase shifts probably have rather wide applicability, for example, to the $3d$ transition metals.

In Sec. III, as an application of the phase-shift parametrization scheme, we develop a semiempirical band structure for silver. To do this, we use a first-principles calculation as a guide, and adjust the parameters specifying the $\eta_l(E)$ to fit Fermi-surface, optical, and photoemission data.

Finally, in Sec. IV, we make some brief concluding remarks about the nature and possible utility of the phase-shift parametrization scheme.

II. DEVELOPMENT OF PARAMETRIZED EXPRESSIONS FOR ENERGY-DEPENDENT PHASE SHIFTS

For the Green's-function (KKR) method, the energy eigenvalues are the solutions of the determinantal equation

$$\det\{B_{ij;l'l'} + \kappa\delta_{il'}\delta_{jj'}\} = 0, \quad (1)$$

where the $B_{ij;l'l'}$ are the energy- and \vec{k} -dependent structure coefficients, and the phase shifts η_l are given by

$$\tan\eta_l = \frac{[R_l(r), j_l(\kappa r)]_{r=r_i}}{[R_l(r), n_l(\kappa r)]_{r=r_i}}, \quad (2)$$

with

$$[R_l(r), j_l(\kappa r)]_{r=r_i} = R_l(r_i) \frac{dj_l(\kappa r)}{dr} \Big|_{r=r_i} - \frac{dR_l(r)}{dr} \Big|_{r=r_i} j_l(\kappa r_i). \quad (3)$$

Here r_i denotes the radius of the inscribed sphere of a muffin-tin potential; $R_l(r)$ is the radial wave function; and $j_l(\kappa r)$ and $n_l(\kappa r)$ are the spherical Bessel and Neumann functions. The energy is given in dimensionless form by ϵ , where

$$E = (2\pi/a)^2\epsilon + V_0, \quad (4)$$

So the zero of ϵ corresponds to the constant potential V_0 between spheres of the muffin-tin potential. For positive ϵ , the quantity κ is proportional to the square root of ϵ ,

$$\kappa = (2\pi/a)\sqrt{\epsilon}, \quad (5)$$

and is appropriately modified⁵ for negative ϵ .

The key step in the phase-shift parametrization scheme is to arrive at functional forms for the ϵ dependence of the $\tan\eta_l$, so that each $\tan\eta_l$ can be specified over a wide range of energy in terms of a few parameters. To do this for the noble metals we are guided by the behavior found in four first-principles calculations performed by Segall, two each for copper⁶ and silver.⁷ For Cu, these calculations were for the "Chodorow potential," for which the $\tan\eta_l$ are shown in Fig. 1, and an l -dependent potential giving the $\tan\eta_l$ shown in Fig. 2. For Ag, the first-principles calculations were for a potential based on Hartree free-ion wave functions giving $\tan\eta_l$ shown in Fig. 3, and for a potential based on Hartree-Fock free-ion wave functions giving $\tan\eta_l$ shown in Fig. 4.

One is much more restricted in the functional forms for the energy dependence of the $\tan\eta_l$ than one might expect at first thought. The basic similarity of the $\tan\eta_l$ behavior in all four cases is evident from an inspection of Figs. 1–4. The behavior of $\tan\eta_0$ shows a marked cusp at $\epsilon=0$ followed by a maximum at positive ϵ . The sign of $\tan\eta_0$ for small $|\epsilon|$ is the same for both positive and negative ϵ . (For the Cu l -dependent potential behavior shown in Fig. 2, in contrast to the other cases $\tan\eta_0$ is negative for small $|\epsilon|$, and instead of having a maximum in $|\tan\eta_0|$ for small positive ϵ , the curve of $\tan\eta_0$ simply levels out into roughly linear behavior.) The $\tan\eta_1$ curves are basically featureless, being rather close to straight-line behavior and changing sign at $\epsilon=0$. The $\tan\eta_2$ curves show a singularity at a value of $\epsilon = \epsilon_0$. This is the so-called

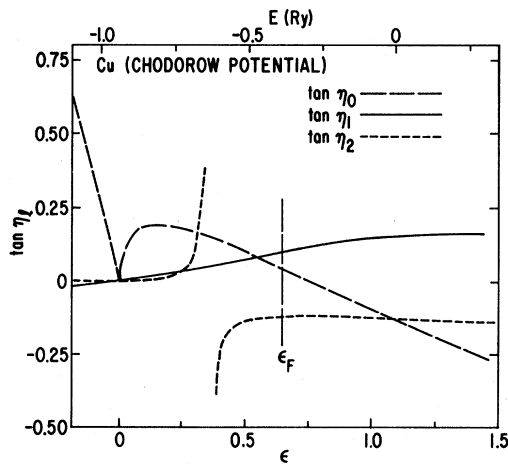


FIG. 1. $\tan \eta_l$'s for Cu Chodorow potential from first-principles calculation (Ref. 6).

"*d*-band resonance," corresponding roughly to the center of the *d* bands. (We note that if one scales ϵ to ϵ_0 , for ϵ/ϵ_0 between 0 and 1, the curves of $\tan \eta_2$ vs ϵ/ϵ_0 are close to identical for all four potentials.) The sign of $\tan \eta_2$ is the same for sufficiently small positive and negative ϵ , but a sign change can occur rather quickly for increasing $|\epsilon|$. One can think of the relative positions of the two most prominent features in the $\tan \eta_l$ behavior, the η_0 cusp and the η_2 singularity, as a measure of the location of the *d* bands relative to the free-electron-like conduction bands.

The final form found for the functional dependence of the $\tan \eta_l$'s on ϵ evolved from trial forms used to

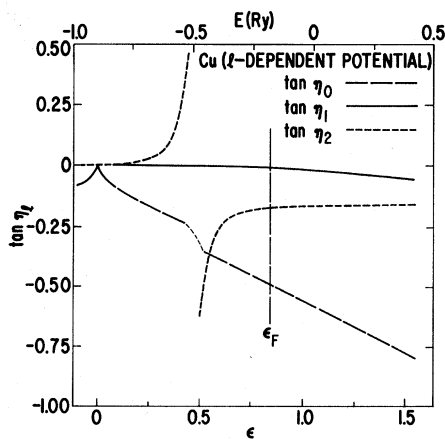


FIG. 2. $\tan \eta_l$'s for a Cu l -dependent potential from first-principles calculation (Ref. 6). (The discontinuity in $\tan \eta_0$ at $\epsilon \sim 0.5$ corresponds to a discontinuity in the potential within r_1 for $l=0$ introduced in the development by Segall of his l -dependent potential.)

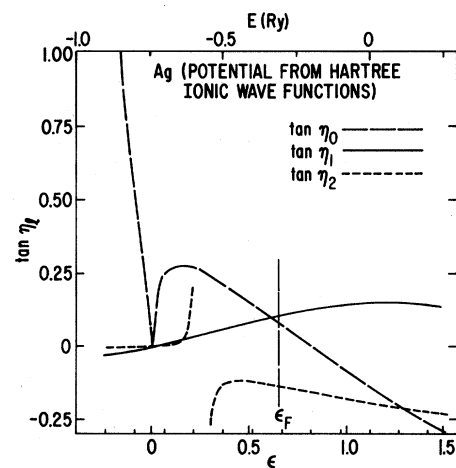


FIG. 3. $\tan \eta_l$'s for Ag potential based on Hartree free-ion wave functions from first-principles calculation (Ref. 7).

match the low- ϵ behavior. The choice of trial forms developed from an examination of the low- ϵ part of the *d*-band structure. This occurred because there is a constraint imposed on the low- ϵ behavior of $\tan \eta_2$ by the low- ϵ behavior of the B_{2020} structure coefficient.⁸ (This structure coefficient enters into the determination of the low-lying *d*-band energies.) This constraint became evident upon studying the X_1 and L_1 energy levels for the Chodorow potential, because these levels fall near $\epsilon = 0$.

The secular determinants giving the X_1 and L_1 energies are of the form

$$0 = \begin{vmatrix} (B_{0000} \tan \eta_0 + 2\pi \sqrt{\epsilon}) & B_{0020} \tan \eta_2 \\ B_{0020} \tan \eta_0 & (B_{2020} \tan \eta_2 + 2\pi \sqrt{\epsilon}) \end{vmatrix}, \quad (6)$$

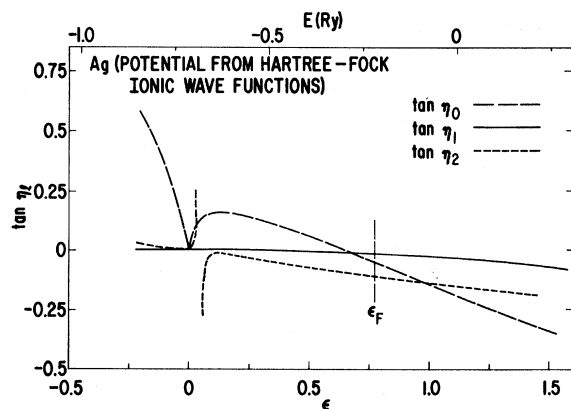


FIG. 4. $\tan \eta_l$'s for Ag potential based on Hartree-Fock free-ion wave functions from first-principles calculation (Ref. 7).

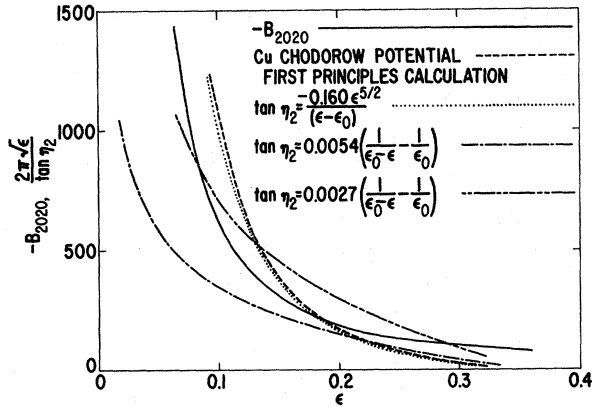


FIG. 5. Approximate solution of Eq. (6) as given by Eq. (7) for $\tan\eta_2$ considering different functions of ϵ . Solutions correspond to intersections of curve for B_{2020} with that for $2\pi(\epsilon)^{1/2}/\tan\eta_2$.

where, of course, the $B_{l, m, m'}$ appropriate to X and to L are to be used. Figure 5 shows the variation of B_{2020} at X for energies in the range where the lower X_1 root occurs. (Similar behavior applies to the lower L_1 root.) The ϵ position for which the determinant in (6) goes to zero (giving the X_1 eigenvalue) is primarily determined by the behavior of the B_{2020} term. Thus, to a good approximation the X_1 energy is determined by the condition

$$B_{2020} = 2\pi\sqrt{\epsilon}/\tan\eta_2. \quad (7)$$

Now, because of the particular energy dependence of B_{2020} , it is not a simple matter to find a form for $\tan\eta_2$ having a "resonant" character and giving one and only one solution for ϵ in (7). For example, the two long dashed curves in Fig. 5 show the difficulties that arise if one tries to use a form

$$\tan\eta_2 = a\left(\frac{1}{\epsilon_0 - \epsilon} - \frac{1}{\epsilon_0}\right).$$

This gives a shallower curve of $\tan\eta_2$ vs ϵ than that obtained from the first-principles theory; and one typically gets either two or no roots rather than one root. On the other hand, a form with $\tan\eta_2 \approx a\epsilon^{5/2}/(\epsilon - \epsilon_0)$ closely follows the first-principles behavior, and gives only one root.

At this point it is useful to consider the leading terms in the series expansions of the Bessel functions entering Eq. (2). For small x ,

$$j_l(x) \sim x^l \quad (8)$$

and

$$n_l(x) \sim x^{-(l+1)}. \quad (9)$$

Then to the extent that the ϵ dependence of the logarithmic derivative can be neglected, we find for

small ϵ that

$$[R_l, j_l(\kappa r)] \sim \kappa^l \sim \epsilon^{1/2}, \quad (10)$$

$$[R_l(r), n_l(\kappa r)] \sim \epsilon^{-(l+1)/2}, \quad (11)$$

and therefore

$$\tan\eta_l \sim \epsilon^{(2l+1)/2}. \quad (12)$$

Thus the behavior $\tan\eta_2 \approx a\epsilon^{5/2}/(\epsilon - \epsilon_0)$ indicated by the discussion in connection with Fig. 5 is just that expected from Eq. (2) if the Bessel functions dominate the ϵ dependence of the $\tan\eta_l$ at low ϵ ; and the factor of $(\epsilon - \epsilon_0)^{-1}$ allows for the presence of the "d-band resonance." The qualitative characteristics of the $\tan\eta_l$ near $\epsilon=0$, noted in the discussion of Figs. 1-4 above, can also be understood on the basis of the dominance of the Bessel functions in that energy regime.

Therefore one is led initially to try the following leading terms:

$$\tan\eta_0 \sim \epsilon^{1/2}, \quad \tan\eta_1 \sim \epsilon^{3/2}, \quad \tan\eta_2 \sim \epsilon^{5/2}/(\epsilon - \epsilon_0). \quad (13)$$

To complete the specification of the functional form of the $\tan\eta_l$, we adopted the empirical procedure of comparing the band structures arising from our parametrized $\tan\eta_l$ to the first-principles results in the four cases corresponding to Figs. 1-4. We used as a rule of thumb the criterion of selecting the simplest form for the $\tan\eta_l$ that would fit all the first-principles energies, across a range of a rydberg or more, with a maximum error of 0.01 Ry for any single energy.

To allow for the possibility of a maximum in $\tan\eta_0$ for increasing ϵ , one has to include a higher-order term in ϵ of competing sign, e.g., $\tan\eta_0 \sim \epsilon^{1/2}(a - b\epsilon)$. It turns out that to get an adequate over-all fit for $\tan\eta_0$ requires a somewhat more complicated form:

$$\tan\eta_0 = s_1|\epsilon|^{1/2}(1 - s_2\epsilon)/(1 + s_3\epsilon) + s_4[1 - \sigma(\epsilon)]|\epsilon|^{3/2}, \quad (14)$$

where

$$\sigma(x) = 0 \text{ for } x < 0 \text{ and } \sigma(x) = 1 \text{ for } x > 0. \quad (15)$$

The final term in (14) is necessary to treat the behavior for negative ϵ . The negative- ϵ behavior is of rather minor consequence in practice since it corresponds to at most the very bottom in energy of the over-all band structure.

Similarly, to describe $\tan\eta_2$ across the entire energy range involves a more complicated form than that given by (13); for d -band metals, we have

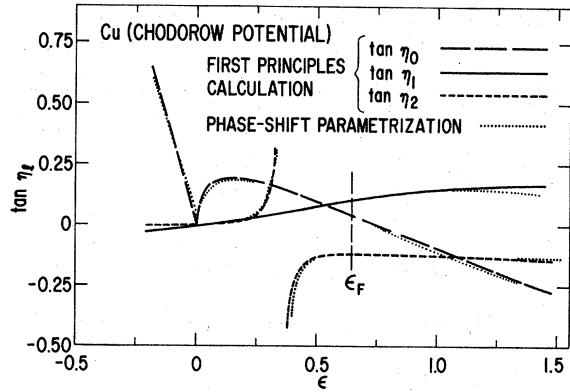


FIG. 6. Comparison of $\tan \eta_i$'s for Cu Chodorow potential from first-principles (Ref. 6) and phase-shift parametrization calculations. (In regions where the phase-shift parametrization results are not shown, the results of the two calculations essentially coincide. Parts of the dotted curves were inadvertently omitted in Ref. 4.) The vertical line labeled ϵ_F indicates the Fermi energy.

(*d*-band metals)

$$\tan \eta_2 = d_2 \frac{|\epsilon|^{5/2}}{\epsilon - d_1} + \sigma(\epsilon - d_1) \left(\frac{d_3}{(\epsilon - d_1)^{1/2}} + d_4 \epsilon^2 \right). \quad (16)$$

Finally, the form of $\tan \eta_1$ can be fit satisfactorily by including the next-order term in ϵ beyond that in (13):

$$\tan \eta_1 = p_1 |\epsilon|^{1/2} (1 - p_2 \epsilon). \quad (17)$$

The absolute value of ϵ is used in several places in (14), (16), and (17) to take account of the negative- ϵ behavior with the greatest simplicity.

Figures 6 and 7 show typical behavior, for Cu and Ag, respectively, for the comparison between the first-principles evaluation of the phase shifts and the fitting by the phase-shift parametrization. The parametrized fitting almost exactly coincides with the first-principles phase shifts except for the few places indicated by a dotted curve.

The values of the ten parameters (four for $\tan \eta_0$, two for $\tan \eta_1$, and four for $\tan \eta_2$) necessary to specify the $\tan \eta_i$, and hence the electron energy-band structure, for the noble metals are given in Table I for the bands corresponding to the Cu Chodorow and "*l*-dependent" potentials and to the Ag potentials coming from Hartree and Hartree-Fock ionic wave functions. (We also include for later reference the parameter values characterizing the semiempirical band structure found for Ag using the phase-shift parametrization technique as described in Sec. III.)

These parameters were obtained by requiring that Eqs. (14), (16), and (17) fit the $\tan \eta_i$ given in the graphs at the appropriate number of ϵ values. The success of this approach relies upon choosing the ϵ 's such that the $(\tan \eta_i, \epsilon)$ pairs represent the key

features of the respective graphs. Initially, the phase shifts for the four potentials (and therefore the parameters in Table I) were examined independently, but the following pattern emerges for all.

For (14), one $(\tan \eta_0, \epsilon)$ pair at $\epsilon < 0$ and three pairs at $\epsilon > 0$ are necessary to fit the parameters. The key features of $\tan \eta_0$ are the nearly linear regions for $\epsilon < 0$ and for $\epsilon > 0.3$, and the maximum in the small positive energy region. Consequently, the ϵ 's for the four pairs are chosen such that $\epsilon_1 = -0.03$ to -0.18 , $\epsilon_2 = 0.05$ to 0.2 (the maximum in $\tan \eta_0$), $\epsilon_3 \approx 0.7$, and $\epsilon_4 \approx 1.4$.

Because $\tan \eta_1$ is nearly linear, the choice of the $(\tan \eta_1, \epsilon)$ pairs for the fitting was not very critical, and these were chosen to be at $\epsilon \approx 0.1$ and 0.9 .

For $\tan \eta_2$, finding the parameters in Eq. (16) requires choosing two points at $\epsilon < \epsilon_0$ and two points at $\epsilon > \epsilon_0$. The key features of the $\tan \eta_2$ behavior are the discontinuity (at ϵ_0) and the near linearity in regions where the effect of the discontinuity becomes small. Since the approximate ϵ_0 was known, one value of $\epsilon > \epsilon_0$ was chosen such that it was quite close to that value of ϵ for which $d(\tan \eta_2)/d\epsilon \approx 0.5$ to 1.0 (i.e., on the "shoulder"—region of maximum curvature—of the $\tan \eta_2$ -vs- ϵ curve); while the second $\epsilon > \epsilon_0$ was chosen at $\epsilon \approx \epsilon_0 + 1.0$, where the $\tan \eta_2$ -vs- ϵ curve is approximately linear. For $\epsilon < \epsilon_0$, the two ϵ 's used were $\epsilon \approx \epsilon_1$ [where ϵ_1 is the value of ϵ at which $d(\tan \eta_2)/d\epsilon_2 = 0.5$, i.e., slightly to the negative side of the low- ϵ shoulder of the $\tan \eta_2$ -vs- ϵ curve] and $\epsilon \approx \epsilon_1 - 0.2$, where the $\tan \eta_2$ -vs- ϵ curve has flattened out.

In Table II, we give a comparison of the energy eigenvalues at some high-symmetry points as calculated directly in the first-principles calculations and from the parametrization scheme. The data of Table II show only a small part of the energies investigated since we looked at about 100 states for \vec{k} both at symmetry points in addition to those shown

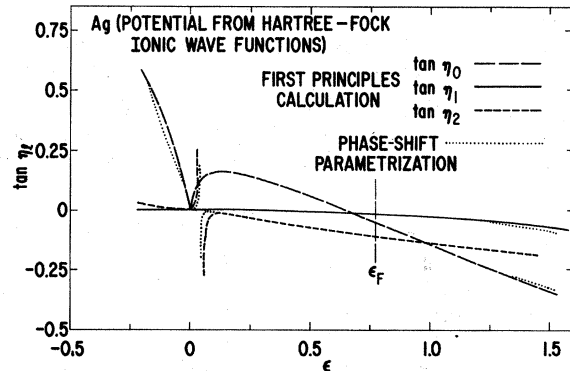


FIG. 7. Comparison of $\tan \eta_i$'s for Ag potential based on Hartree-Fock free-ion wave functions from first-principles (Ref. 7) and phase-shift parametrization calculations.

TABLE I. Parameters entering expressions for $\tan\eta_i$ given by Eqs. (14) and (16)–(18) of text.

	s_1	s_2	s_3	s_4^a	p_1
Cu (Chodorow)	0.767	1.331	1.552	0.550	0.300
Cu (l dependent)	0.279	-0.801	0.062	...	-0.019
Ag (Hartree)	1.170	1.240	2.270	2.240	0.331
Ag (Hartree-Fock)	0.660	1.560	1.550	0.620	0.020
Ag (semiempirical phase-shift parametrization)	1.555	1.590	1.563	-6.780	-0.087
Al	4.176	0.607	5.800	2.000	0.720
	p_2	d_1	d_2	d_3	d_4
Cu (Chodorow)	0.520	0.360	-0.160	0.015	0.105
Cu (l dependent)	-0.093	0.468	-0.158	0.015	0.107
Ag (Hartree)	0.595	0.250	-0.212	0.001	0.104
Ag (Hartree-Fock)	2.300	0.024	-0.300	0	0.166
Ag (semiempirical phase-shift parametrization)	1.025	0.173	-0.336	0.011	0.198
Al	0.390	...	0.100	...	-0.024

^aFor Cu with the l -dependent potential, all band energies occur for positive ϵ . Thus no value of s_4 is required.

in Table II and also along symmetry axes. Actually, we did not quite achieve the goal of no departure from the first-principles calculations greater than 0.01 Ry. Typically, for a few energies at the top of the range considered, roughly a rydberg above Γ_1 , the error somewhat exceeded this. (This energy region where the departure exceeds 0.01 Ry corresponds to the high- ϵ region in Figs. 6 and 7 where the parametrized phase shifts given by the dotted curves deviate significantly from the first-principles values.) However, the root-mean-square deviation was very much smaller than 0.01 Ry.

We have also parametrized the phase shifts in the case of a simple (nearly free-electron-like) metal.

This has been done by retaining the same expressions for $\tan\eta_0$ and $\tan\eta_1$ as for the noble metals. For $\tan\eta_2$, the resonant character has been eliminated, and for positive ϵ we have used $\tan\eta_2 \sim \epsilon^{5/2}$. [This amounts to multiplying the expression in (16) by $(\epsilon - d_1)$. However, for negative ϵ , we find it necessary only to retain the ϵ^2 term resulting from this multiplication.] For simple metals, we find

$$\text{(simple metals)} \quad \tan\eta_2 = d_2 |\epsilon|^{5/2} + \sigma(\epsilon) d_4 \epsilon^3. \quad (18)$$

Thus for Al we use (14), (17), and (18) to find the parametrized phase shifts. The phase-shift parameters for Al, obtained by fitting the phase shifts in

TABLE II. Energies (in Ry) at high-symmetry points from first-principles (fp) and phase-shift parametrization (psp) calculations.

State	Cu Chodorow potential		Cu l -dependent potential		Ag potential from Hartree wave functions		Ag potential from Hartree-Fock wave functions		Al	
	fp	psp	fp	psp	fp	psp	fp	psp	fp	psp
Γ_1	-1.043	-1.043	-0.836	-0.831	-0.857	-0.852	-0.781	-0.787	-0.463	-0.462
Γ_{12}	-0.584	-0.577	-0.433	-0.434	-0.522	-0.522	-0.654	-0.653
$\Gamma_{25'}$	-0.644	-0.638	-0.505	-0.506	-0.590	-0.592	-0.703	-0.693
L_1	-0.778	-0.787	-0.646	-0.652	-0.706	-0.703	-0.806	-0.802
L_3	-0.648	-0.644	-0.511	-0.511	-0.594	-0.588	-0.729	-0.728
L_3	-0.539	-0.534	-0.380	-0.379	-0.468	-0.469	-0.602	-0.600
L_2'	-0.422	-0.421	-0.247	-0.244	-0.342	-0.346	-0.222	-0.224	0.020	0.027
L_1	-0.081	-0.076	0.189	0.192	-0.026	-0.026	-0.035	-0.035	0.049	0.051
X_1	-0.781	-0.791	-0.666	-0.673	-0.717	-0.711	-0.829	-0.819
X_3	-0.745	-0.754	-0.630	-0.633	-0.693	-0.689	-0.823	-0.814
X_2	-0.541	-0.538	-0.383	-0.383	-0.472	-0.472	-0.604	-0.609
X_5	-0.526	-0.525	-0.366	-0.366	-0.453	-0.453	-0.585	-0.588
X_4'	-0.224	-0.218	-0.029	-0.023	-0.184	-0.183	-0.051	-0.050	0.159	0.167
X_1	0.169	0.173	0.389	0.392	0.196	0.196	0.175	0.169	0.235	0.239

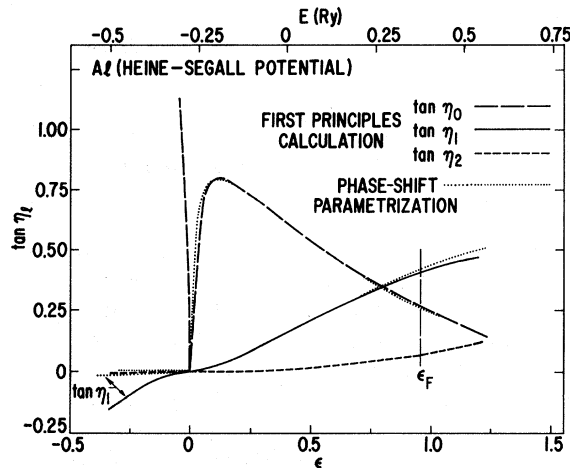


FIG. 8. Comparison of $\tan \eta_i$'s for Al from first-principles (Ref. 8) and phase-shift parametrization calculations.

Segall's first-principles calculation,⁹ are listed in Table I; and in Fig. 8, the corresponding phase shifts given by (14), (17), and (18) are compared to the values for the first-principles calculation. Also, a comparison of the band energies for Al at high-symmetry points from the first-principles and phase-shift parametrization calculations is included in Table II.

One could use simpler approximations than those of (14), (16), and (17) if one were willing to surrender accuracy and/or restrict oneself to a smaller energy range. For example, one could use a straight-line fit to $\tan \eta_1$ as an approximation to the curve given by (17).

III. SEMIEMPIRICAL DETERMINATION OF SILVER BAND STRUCTURE BY PHASE-SHIFT PARAMETRIZATION TECHNIQUE

The phase-shift parametrization (PSP) scheme can be readily employed in the case where, on the basis of a first-principles calculation, one has a good semiquantitative guide to the η_i behavior. Adjustments would then be made to bring about accord with available experimentally determined data on the electronic structure. Once the parametric forms of the $\tan \eta_i$, such as (14), (16), and (17), have been determined, the PSP scheme is particularly flexible with regard to the amount of empirical data that can be incorporated. One could make very minor adjustments to a first-principles calculation, or one could develop a substantially experimentally determined band structure. In this section, by considering the behavior of silver, we shall illustrate the use of the PSP scheme to substantially adjust a first-principles band calculation by the use of experimental data. This amounts to modifying the original potential by the introduction of experi-

mental data.

The early band calculations for Ag done by Segall⁷ showed that the principal difficulty in obtaining satisfactory results was in properly positioning the d bands with respect to the more free-electron-like conduction bands. There have been suggestions¹⁰ for shifting the d bands upward from the value found in Segall's calculation (using a potential determined from Hartree-Fock free-ion wave functions) in some fairly crude way in order to get agreement with experimental optical or photoemission data. The phase-shift parametrization technique offers a particularly elegant and physically reasonable way of making this sort of correction to a first-principles calculation by use of empirical data. Indeed, using the phase-shift parametrization technique, one can blend a good deal of experimental information into the framework of a first-principles calculation. Table III gives an outline of the way we have done this for Ag using Segall's calculations (for a potential determined from Hartree-Fock free-ion wave functions) as a starting point.

Since there are a substantial number of parameters in the expressions for $\tan \eta_0$, $\tan \eta_1$, and $\tan \eta_2$ [given by (14), (16), and (17), respectively], the values of which are to be determined, there is a correspondingly substantial number of steps and pieces of data to be used in the fitting. If one were willing to accept a band structure with less over-all accuracy, one could use simpler forms involving fewer parameters for the $\tan \eta_i$, and hence need fewer data and steps in the process of evaluating the parameters.

Table III shows the combination of types of experimental data and first-principles calculational results used in the parametrization procedure. The label η_i at the end of most lines indicates the phase shift about which that step provides information. (In Table III, and the associated discussion below,

TABLE III. Semiempirical phase-shift parametrization scheme for silver.

(a)	$E(L_{2'})$ from Segall's Hartree-Fock (Ref. 7), η_1
(b)	Set E_F , from Fermi-surface analysis (Ref. 10) and photoemission data (Ref. 11): $E_F = E(L_{2'}) + 0.3$ eV
(c)	$E(L_{3 \text{ upper}}) = E_F - 3.9$ eV, optical (Ref. 10), η_2
(d)	$E(X_3) = E(L_{3 \text{ upper}}) - 3.5$ eV, photoemission (Ref. 12), η_2
(e)	$E(\Gamma_{25'}) - E(X_3)$ from (Ref. 7) Ag H-F $\rightarrow E(\Gamma_{25'})$, η_2
(f)	$E(X_{4'})$, optical (Ref. 10), $\eta_1 \rightarrow \eta_1$ completely determined
(g)	Belly radii (Ref. 13) η_0, η_2 at $E_F \rightarrow \eta_2$ completely determined
(h)	$E(\Gamma_1)$ from (Ref. 7) Ag H-F, η_0
(i)	$E(L_{1 \text{ upper}})$ photoemission (Ref. 11), η_0
(j)	$E(W_{1 \text{ lower}})$, relative position in d bands (Ref. 7), $\eta_0 \rightarrow \eta_0$ completely determined
(k)	Checks: neck radius (Ref. 13), $E(X_4) - E(X_1)$ optical (Ref. 14), self-consistency of E_F

"Hartree-Fock" or "H-F" is used to denote the results of Segall's calculation⁷ using a potential based on Hartree-Fock free-ion wave functions.) We now present a detailed discussion of the parametrization procedure following the steps listed in Table III.

First we note that, strictly speaking, there are 11 rather than 10 parameters in our scheme. This is because the constant potential between spheres of the muffin tin [i. e., V_0 of (4)] which sets the zero of ϵ is also a parameter. We choose this as the value in Segall's first-principles H-F calculation. So the relationship between E and ϵ is for Ag

$$\epsilon = (E + 0.7126)/0.6396 \quad (19)$$

with E in Ry.

The steps in the parametrization procedure follow where the numbers correspond to those in Table III:

(a) Take $E(L_{2'})$ from Segall's H-F band calculation. (The $L_{2'}$ state is a pure p state, i. e., only $\tan\eta_1$ enters into the energy determination.)

The most conspicuous feature of the s and p conduction-band behavior from the phase-shift point of view is that $\tan\eta_0$ and $\tan\eta_1$ both go to zero as ϵ goes to zero. Thus, matching the $L_{2'}$ energy to the first-principles H-F result and choosing the scale of ϵ as in (19) basically sets the over-all scale of conduction-band behavior from the phase-shift point of H-F calculation.

The $L_{2'}$ energy is given by

$$L_{2'}, 0 = B_{1111} \tan\eta_1 + 2\pi\sqrt{\epsilon} \quad (20)$$

From H-F, $E(L_{2'}) = -0.222$ Ry, so that from (19), $\epsilon(L_{2'}) = 0.767$. Thus, using the value for the structure coefficient at this ϵ in (20) gives

$$\tan\eta_1(\epsilon = 0.767) = -0.01251 \quad (21)$$

(b) We take the value of $E_F - E(L_{2'})$ from photoemission data¹¹:

$$E_F = E(L_{2'}) + 0.3 \text{ eV} \rightarrow E_F = -0.200 \text{ Ry} \quad (22)$$

(One can obtain¹⁰ the same energy difference from the experimentally determined neck radius and neck mass.) This gives

$$\epsilon_F = 0.8014 \quad (23)$$

and effectively places the Fermi energy relative to the conduction bands.

(c) Choose $E(L_{32})$ (the upper L_3 energy—a purely d -like state) by requiring that the difference between the Fermi energy and the top of the d -band complex as given by $E(L_{32})$ gives the experimental value for the optical interband edge

$$E_F = E(L_{32}) + 3.97 \text{ eV} \rightarrow E(L_{32}) = -0.492 \text{ Ry} \quad (24)$$

This step essentially sets the d -band energies relative to the conduction bands using the same physical criterion as that in the paper of Cooper, Ehrenreich,

and Philipp.¹⁰

The L_3 energy is given by the determinantal equation

$$L_3, 0 = \begin{vmatrix} (B_{2121} \tan\eta_2 + 2\pi\sqrt{\epsilon}) & B_{2122} \tan\eta_2 \\ B_{2122} \tan\eta_2 & (B_{2222} \tan\eta_2 + 2\pi\sqrt{\epsilon}) \end{vmatrix} \quad (25)$$

Equation (25) gives a quadratic equation for $\tan\eta_2$ at $\epsilon(L_{32}) = 0.345$. However, it is simple to select the physically meaningful root of the quadratic equation. First, we note that one root falls very close to the value given by the sign change of $B_{2121} + 2\pi\sqrt{\epsilon}/\tan\eta_2$, and for all of the first-principle calculations that have been considered the L_{32} root was very closely given by that sign change. Second, the discarded root would lead to a singularity in $\tan\eta_2$, i. e., the " d -band resonance," above the L_{32} energy. This would be physically meaningless since the d -band resonance falls in the middle of the d -band complex, and the L_{32} energy is at the top.

Choosing the appropriate root of (25) gives

$$\tan\eta_2(\epsilon = 0.345) = -0.085120 \quad (26)$$

(d) Take

$$E(L_{32}) - E(X_3) = 3.5 \text{ eV} \quad (27)$$

from the photoemission measurement¹² of the d -band width in Ag. Here X_3 is a purely d -like state at the bottom of the d -band complex.

Since $E(L_{32})$ is given by (c), this yields

$$E(X_3) = -0.749 \text{ Ry} \rightarrow \epsilon(X_3) = -0.057 \quad (28)$$

Using the fact that $\epsilon(X_3)$ is the root of

$$X_3, 0 = B_{2222} \tan\eta_2 + 2\pi\sqrt{\epsilon} \quad (29)$$

this gives

$$\tan\eta_2(\epsilon = -0.057) = 0.001137 \quad (30)$$

(e) Take $E(\Gamma_{25'}) - E(X_3) = 0.120$ Ry from the first-principles H-F calculation. Since $E(X_3)$ is already known from (d), this gives

$$E(\Gamma_{25'}) = -0.629 \text{ Ry} \rightarrow \epsilon(\Gamma_{25'}) = 0.131 \quad (31)$$

(Physically, this means that we are taking the width of the lowest d band from the H-F calculation.)

Since $(\Gamma_{25'})$ is given by

$$\Gamma_{25'}, 0 = B_{2222} \tan\eta_2 + 2\pi\sqrt{\epsilon} \quad (32)$$

this yields

$$\tan\eta_2(\epsilon = 0.131) = 0.050323 \quad (33)$$

(f) Take $E(X_5) - E(L_{32}) = 0.017$ Ry from the H-F calculation. This is a very small number since the topmost d band is almost flat; and since $E(L_{32})$ is known from (c), this serves to determine $E(X_5)$:

$$E(X_5) = -0.475 \text{ Ry} \quad (34)$$

From the optical data,¹⁰

$$E(X_{4'}) - E(X_5) = 5.5 \text{ eV} \quad (35)$$

so that

$$E(X_{4'}) = -0.071 \text{ Ry} \rightarrow \epsilon(X_{4'}) = 1.003. \quad (36)$$

$X_{4'}$ is a purely p -like state given by

$$X_{4'}, 0 = B_{1010} \tan \eta_1 + 2\pi \sqrt{\epsilon}, \quad (37)$$

and using the known values of the structure coefficient

$$\tan \eta_1 (\epsilon = 1.003) = 0.002468. \quad (38)$$

Steps (a) and (f) give $\tan \eta_1$ at $\epsilon = 0.767$ and $\epsilon = 1.003$, respectively. This allows us to evaluate the two parameters p_1 and p_2 in Eq. (17), which determine the behavior of $\tan \eta_1$. The values found are

$$\Delta_1, 0 = \begin{vmatrix} (B_{0000} \tan \eta_0 + 2\pi \sqrt{\epsilon_F}) & B_{1000} \tan \eta_1 & B_{2000} \tan \eta_2 \\ B_{1000} \tan \eta_0 & (B_{1010} \tan \eta_1 + 2\pi \sqrt{\epsilon_F}) & B_{2010} \tan \eta_2 \\ B_{2000} \tan \eta_0 & B_{2010} \tan \eta_1 & (B_{2020} \tan \eta_2 + 2\pi \sqrt{\epsilon_F}) \end{vmatrix}. \quad (40)$$

The $\langle 110 \rangle$ belly radius corresponds to the values of $\tan \eta_0$, $\tan \eta_1$, and $\tan \eta_2$ at ϵ_F satisfying the 4×4 determinantal equation giving the Σ_1 band energies:

$$\Sigma_1, 0 = \begin{vmatrix} (B_{0000} \tan \eta_0 + 2\pi \sqrt{\epsilon_F}) & B_{1000} \tan \eta_1 & B_{2000} \tan \eta_2 & B_{2200} \tan \eta_2 \\ B_{1000} \tan \eta_0 & (B_{1010} \tan \eta_1 + 2\pi \sqrt{\epsilon_F}) & B_{2010} \tan \eta_2 & B_{2210} \tan \eta_2 \\ B_{2000} \tan \eta_0 & B_{2010} \tan \eta_1 & (B_{2020} \tan \eta_2 + 2\pi \sqrt{\epsilon_F}) & B_{2220} \tan \eta_2 \\ B_{2200} \tan \eta_0 & B_{2210} \tan \eta_1 & B_{2220} \tan \eta_2 & (B_{2222} \tan \eta_2 + 2\pi \sqrt{\epsilon_F}) \end{vmatrix}. \quad (41)$$

Now since ϵ_F and the belly radii are specified, all the structure coefficients $B_{im'm'}$ in (40) and (41) have specified values. Also the value of $\tan \eta_1$ at ϵ_F is specified. Thus (40) and (41) give two fairly complicated equations specifying $\tan \eta_0$ and $\tan \eta_2$ at ϵ_F . The easiest way to solve these equations is to feed a set of values of $\tan \eta_0$ into (40) and solve for $\tan \eta_2$. The result of doing this is shown as the dashed curves in Fig. 9. Then one can feed $\tan \eta_2$ values into (41) and solve for $\tan \eta_0$ as shown in the solid curves of Fig. 9. There is only one set of values of $\tan \eta_0$ and $\tan \eta_2$ at ϵ_F simultaneously satisfying (40) and (41), i. e., giving an intersection between the dashed and solid curves of Fig. 9. (Note that while the curves approach each other closely in the upper-right quadrant of Fig. 9, they do not cross. The only crossing is in the lower-left quadrant. This result was investigated with great care.) These values are

$$\begin{aligned} \tan \eta_0 (\epsilon_F = 0.8014) &= -0.1264, \\ \tan \eta_2 (\epsilon_F = 0.8014) &= -0.1655. \end{aligned} \quad (42)$$

From (c)–(e) and (g), one has the value of $\tan \eta_2$

listed in Table I.

(g) Determine $\tan \eta_0$ and $\tan \eta_2$ at ϵ_F to match the experimentally measured $\langle 100 \rangle$ and $\langle 110 \rangle$ belly radii. In the analysis we use the values for the belly radii found in Roaf's analysis of Shoenberg's de Haas–van Alphen data.¹³ These are

$$k_{\langle 100 \rangle \text{ belly}} = 0.8043 \times 2\pi/a, \quad (39)$$

$$k_{\langle 110 \rangle \text{ belly}} = 0.7542 \times 2\pi/a.$$

(These values differ somewhat from those found by Bohm and Easterling¹⁵ and by Morse¹⁶ using the magnetoacoustic effect.)

The $\langle 100 \rangle$ belly radius corresponds to the values of $\tan \eta_0$, $\tan \eta_1$, and $\tan \eta_2$ at ϵ_F satisfying the 3×3 determinantal equation giving the Δ_1 band energies:

at $\epsilon = 0.345$, $\epsilon = -0.057$, $\epsilon = 0.131$, and $\epsilon_F = 0.8014$, respectively. This allows one to determine values of the four parameters in the expression for $\tan \eta_2$ of Eq. (14), and these values are listed in Table I.

(h) Take the value of $E(\Gamma_1)$ (a pure s -like state) as given by Segall's H-F calculation. [This is used only to evaluate the parameter s_4 in (12), which is relevant only to the small part of the band structure where ϵ is negative.] We have

$$E(\Gamma_1) = -0.781 \text{ Ry} \rightarrow \epsilon(\Gamma_1) = -0.1069. \quad (43)$$

Since $\epsilon(\Gamma_1)$ is given by

$$\Gamma_1, 0 = B_{0000} \tan \eta_0 + 2\pi \sqrt{|\epsilon|}, \quad (44)$$

then

$$\tan \eta_0 (\epsilon = -0.1069) = 0.2936. \quad (45)$$

(i) We use the value of $E(L_{1 \text{ upper}})$ obtained using photoemission data to determine $\tan \eta_0$ at $L_{1 \text{ upper}}$.

Berglund and Spicer¹¹ have found structure in the photoemission electron-energy-distribution data that they attribute to direct transitions from L_2 to L_1 with an energy difference of 4.2 eV. This would put L_1 3.9 eV above E_F . However, $E(L_1) - E_F$ cannot be less than the optical onset frequency for interband transitions which we take as 3.97 eV. Clearly, the

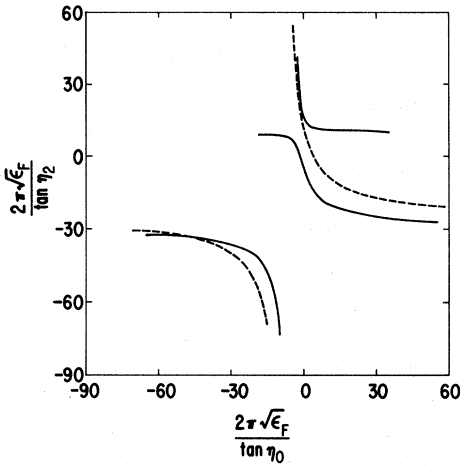


FIG. 9. Determination of values of $\tan\eta_0$ and $\tan\eta_2$ satisfying Eqs. (40) and (41) and giving experimental belly radii.

energy from E_F up to L_1 is about the same as that down to the top of the d bands, so we take these to coincide and put

$$E(L_{1 \text{ upper}}) - E_F = 3.97 \text{ eV} . \quad (46)$$

This gives

$$E(L_{1 \text{ upper}}) = 0.092 \text{ Ry} \rightarrow \epsilon(L_{1 \text{ upper}}) = 1.258 . \quad (47)$$

The determinantal equation yielding $\epsilon(L_1)$ is

$$L_1, 0 = \begin{vmatrix} (B_{0000} \tan\eta_0 + 2\pi\sqrt{\epsilon}) & B_{2000} \tan\eta_0 \\ B_{2000} \tan\eta_2 & (B_{2020} \tan\eta_2 + 2\pi\sqrt{\epsilon}) \end{vmatrix} . \quad (48)$$

Since the value of $\tan\eta_2$ has already been determined for all ϵ , this allows us to find

$$\tan\eta_0(\epsilon = 1.258) = -0.43758 . \quad (49)$$

(j) From (g) and (i) we have the value of $\tan\eta_0$ at two positive values of ϵ . To evaluate s_1 , s_2 , and s_3 in (12) it is necessary to specify $\tan\eta_0$ at a third positive value of ϵ . It is convenient to do this for a value of ϵ falling near the maximum in $\tan\eta_0$, so that one gets physically reasonable behavior for the parametrized $\tan\eta_0$ at that maximum. Such a value of ϵ falls in the middle of the d -band complex where the energy-band behavior is insensitive to the detailed behavior of $\tan\eta_0$. Thus any reasonable way of determining $\tan\eta_0$ in this ϵ regime will suffice.

To do this we considered the energy W_1 falling in the middle of the d -band complex, and specified by the determinantal equation

$$W_1, 0 = \begin{vmatrix} (B_{0000} \tan\eta_0 + 2\pi\sqrt{\epsilon}) & B_{2000} \tan\eta_2 \\ B_{2000} \tan\eta_0 & (B_{2020} \tan\eta_2 + 2\pi\sqrt{\epsilon}) \end{vmatrix} . \quad (50)$$

Now in the two first-principles Ag band calculations performed by Segall⁷ (that for a potential based on

Hartree-Fock free-ion wave functions already referred to as "H-F," and that for a potential based on Hartree free-ion wave functions, referred to as "H" here), the W_1 energy fell very close to halfway between the two L_3 , purely d -like energies. For H, W_1 lay 0.01 above the halfway point between $\epsilon(L_{31})$ and $\epsilon(L_{32})$, and for H-F, W_1 lay 0.02 above the halfway point. If we regard the relative position of W_1 in the d -band complex as a feature of the band structure to be preserved, then the average of the H-F and H behaviors leads us to set the W_1 value of ϵ at 0.015 above the halfway point between $\epsilon(L_{31})$ and $\epsilon(L_{32})$, so

$$\epsilon(W_1) = 0.250 , \quad (51)$$

and from (50)

$$\tan\eta_0(\epsilon = 0.250) = 0.250 . \quad (52)$$

Actually, the rather cumbersome procedure described above gives a maximum value of $\tan\eta_0$ almost exactly coinciding with that from the first-principles H-F calculation. Since all we really care about with regard to the evaluation of $\tan\eta_0$ for ϵ in the middle of the d -band complex is that the maximum of $\tan\eta_0$ behaves reasonably (i. e., $\tan\eta_0$ does not go to some extraordinarily large value), the criterion used here and yielding (52) is quite sufficient.

From the steps (g)–(j) we have the value of $\tan\eta_0$ at four values of ϵ . This allows us to determine the values for the parameters s_1 , s_2 , s_3 , and s_4 listed in Table I.

This completes the determination of $\tan\eta_0$, $\tan\eta_1$, and $\tan\eta_2$. We emphasize the difference in importance between the various constraints on the phase-shift parameters treated in steps (a)–(j). For example, the constraint of step (c), which in effect sets the energy of the d bands with respect to the conduction bands, is physically the most important constraint introduced in our analysis, while step (j) introduces a very loose and rather unimportant constraint. We feel that the use of physical judgment in selecting the constraints, and in effect assigning their importance, is a strength of the present analysis scheme.

Figure 10 shows this phase-shift behavior obtained from our semiempirical scheme compared to that from Segall's⁷ H-F calculation. The most conspicuous change is the shift of the d -band resonance for the phase-shift parametrization calculation to higher energies relative to the well-defined features of the conduction-band shifts.

Once the phase shifts have been fully determined, the band energies can be calculated at a number of points in the usual way. These are tabulated for the high-symmetry points in Table IV. The energies of a number of additional states along symmetry axes have also been calculated, and the band

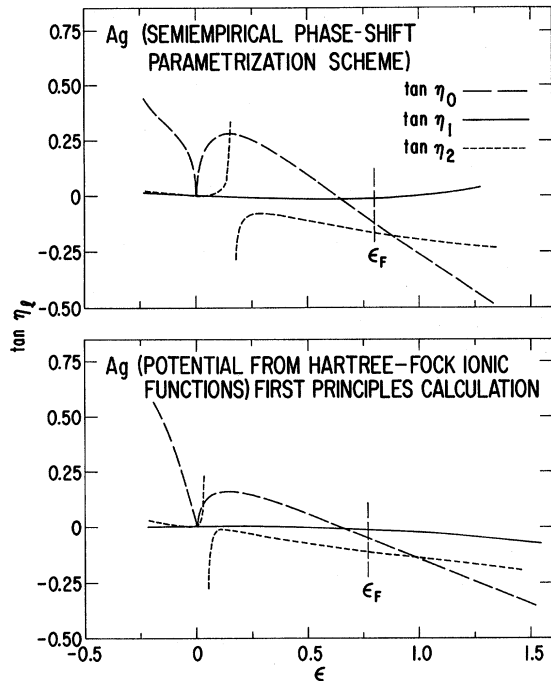


FIG. 10. Comparison of $\tan \eta_i$'s for Ag obtained by the semiempirical phase-shift parametrization scheme of Table III with those for first-principles calculation (Ref. 7) with potential based on Hartree-Fock free-ion wave functions.

structure is shown in Fig. 11.

(k) As a check on the reasonableness of our Ag band structure, we have calculated several quantities.¹⁷ First, we have found a neck radius

$$|k_x|_{\epsilon_F} = (0.109 \pm 0.001) \times 2\pi/a.$$

This compares to the experimental values of $0.107 \times 2\pi/a$ obtained by Roaf in analyzing Shoenberg's de Haas-van Alphen data,¹³ and the value $0.111 \times 2\pi/a$ found by Bohm and Easterling¹⁵ from the magnetoacoustic effect.

Second, Ehrenreich and Philipp¹⁴ have tentatively identified optical structure associated with the energy difference $E(X_4) - E(X_1)$. Their data give this difference as 0.684 Ry, while the present calculation gives 0.678 Ry.

Finally, we have checked the self-consistency of the Fermi energy used. For the band structure of Fig. 11, by counting states using the approximate method used by Segall in his Cu calculations,⁶ we find $E_F = -0.207$ Ry. Considering the numerical accuracy of the calculations (especially the approximation⁶ used to calculate E_F), this is in reasonable agreement with the value of -0.200 Ry found in step (b).

IV. CONCLUDING REMARKS

Since we have fed in some of the experimental

data, our calculation has a great built-in agreement with key experimental features over an energy range of almost a rydberg. For example, it is important to obtain the correct energy separation between the highest d band and the Fermi level and also between the Fermi level and the upper (unoccupied) L_1 and X_1 states in order to give the proper onset of the interband optical transitions. These features of the electronic structure, and others that are essentially tied to them, are uncertain in an *a priori* calculation because of the well-known "sensitivity" of the d bands to small changes in the potential, but they are properly given in our calculation, as illustrated in Fig. 12, by the appropriate use of empirical data. In Fig. 12, for comparison, the results of Segall's H and H-F calculations are also shown. The band energies have been plotted holding the $L_{2'}$ energy fixed. The present d -band-to- $L_{2'}$ energy difference is intermediate to the H value that was too small and the H-F value that was too large.

In addition to the early work of Segall,⁷ there have been several other calculations¹⁸⁻²¹ of the band structure of silver. One of these, by Lewis and Lee,²¹ was an interpolation calculation based on Mueller's² method; three of the others were first-principles calculations; and the calculation of Jacobs²² combined a largely first-principles calculation for a limited number of states with an interpolation calculation.

Lewis and Lee selected 19 energy levels at Γ , X , L , and W from Segall's H calculation. Those levels identified as d levels were then shifted down in energy to give the correct optical interband edge; and the 10 parameters of the Mueller scheme were obtained by fitting the 19 energies with an rms deviation of 0.016 Ry. Thus Lewis and Lee made

TABLE IV. Energies (in Ry) at high-symmetry points for Ag from semiempirical phase-shift parametrization scheme outlined in Table III.

State	Energy (Ry)	State	Energy (Ry)
Γ_1	-0.781	K_1	-0.688
$\Gamma_{25'}$	-0.626	K_1	-0.631
Γ_{12}	-0.556	K_3	-0.560
		K_4	-0.538
X_1	-0.763	K_2	-0.497
X_3	-0.748	K_3	0.082
X_2	-0.497	K_1	0.159
X_5	-0.473		
X_4'	-0.075	$W_{2'}$	-0.701
X_1	0.296	W_3	-0.640
		W_1	-0.553
L_1	-0.743	$W_{1'}$	-0.473
L_3	-0.634	W_3	0.180
L_3	-0.492	$W_{2'}$	0.292
$L_{2'}$	-0.222	W_1	0.425
L_1	0.092		

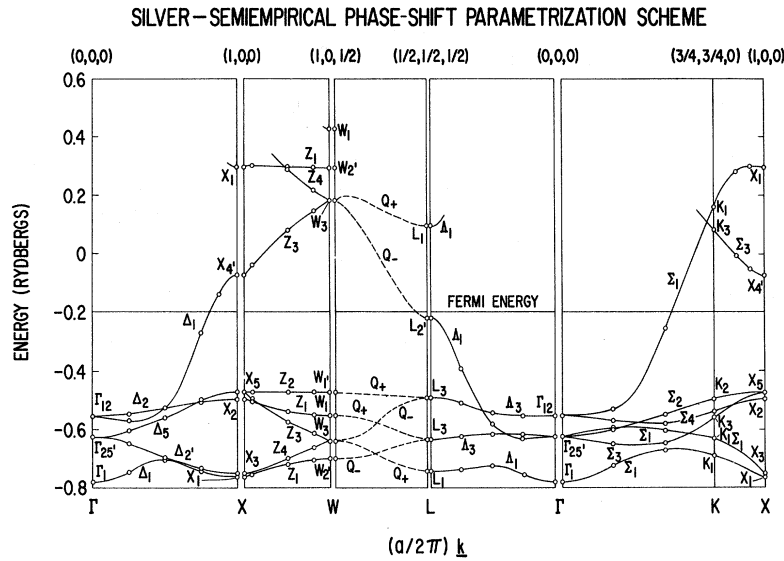


FIG. 11. Calculated energy bands for Ag along the various symmetry axes in the Brillouin zone and on the zone surface. These have been obtained by the semiempirical phase-shift parametrization scheme outlined in Table III and were calculated using the phase shifts of Fig. 10.

no such comprehensive attempt as the present work to adjust the first-principles results by using empirical data.

Jacobs²² first used a calculation based on the earlier model Hamiltonian work, for nontransition metals, of Heine and co-workers²³ to calculate the energies at twelve points in the Brillouin zone along symmetry axes and at points of high symmetry. This calculation differed from a strictly first-principles calculation in choosing the core potential to fit ionic energy levels. Jacobs then used a model Hamiltonian interpolation scheme similar to those of Ehrenreich and Hodges¹ and of Mueller² to find energies throughout the Brillouin zone. Without further empirical adjustment (such as Jacobs²² did for Cu and Au), the results of this calculation do not give sufficiently accurate agreement with the experimentally indicated energy differences. For example, the $L_{2'}$ -upper- L_3 energy

difference is calculated as 0.325 Ry, while the experimental value [see (a) and (c) of Sec. III] is 0.270 Ry.

Of the three first-principles calculations,¹⁸⁻²⁰ those by Snow¹⁸ and by Christensen¹⁹ give results that are most reasonable in comparison with experiment. In Table V, we compare our results with the results of those calculations for some energy differences giving the width of the sp band and d band and their relative positions with respect to each other and to the Fermi energy. Of Snow's two calculations, the one using $\frac{5}{6}$ of the Slater-exchange term gives results closer to experiment, and we will restrict our discussion to that calculation. Christensen actually investigated the band structures for seven different potentials, and selected the "best" one on the empirical basis of agreement with the experimental data. (This was for his potential labeled V_1 based on relativistic Dirac-Slater

TABLE V. Ag energy-state differences (in Ry).

	$\Gamma_{25'} - \Gamma_1$	$X_5 - \Gamma_1$	$X_5 - X_1$	$X_{4'} - \Gamma_1$	$E_F - X_5$	$E_F - L_3$	$E_F - L_{2'}$	$L_1 - L_{2'}$
Segall:								
Hartree	0.267	0.404	0.264	0.673	0.143	0.158	0.032	0.316
Hartree-Fock	0.078	0.196	0.244	0.730	0.365	0.382	0.002	0.187
Snow:								
Slater = 1	-0.011	0.105	0.198	0.665	0.387	0.400	-0.013	...
Slater = $\frac{5}{6}$	0.090	0.221	0.235	0.667	0.290	0.304	0.007	...
Christensen:	0.104	0.227	0.235	0.671	0.304	0.302	0.022	0.319
V_1 potential								
Present calc semiempirical phase-shift parametrization	0.155	0.308	0.290	0.706	0.266	0.292	0.022	0.314

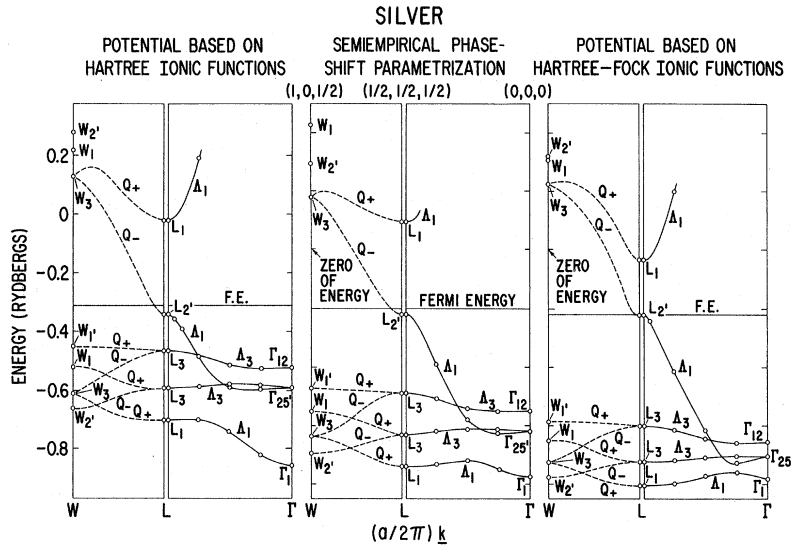


FIG. 12. Comparison of Ag band structure near symmetry point L in Brillouin zone for semiempirical phase-shift parametrization calculation with those from first-principles calculation (Ref. 7) with potentials based on Hartree and on Hartree-Fock free-ion wave functions.

atomic calculations with full Slater exchange in both the atomic and crystal calculations.) So in a sense his work amounts to a semiempirical fitting scheme, however, not a systematic one. (Note that Christensen's best results are for full Slater exchange, while Snow's best results are for $\frac{5}{8}$ of the Slater-exchange term.) As already pointed out, our bands give excellent agreement with the experimental neck radius. This is also true for Christensen's V_1 potential, but Snow's value for the neck radius is only about $\frac{2}{3}$ of the experimental value. (Also, unfortunately Snow's band calculations do not extend to high enough energy to give the behavior of the upper- L_1 energy.) As shown in Table V, both Snow's $\frac{5}{8}$ Slater-exchange results and those for Christensen's V_1 potential are intermediate between Segall's H-F and the present results at the lower energies, and are close to the present semiempirical phase-shift parametrization results for energies near the Fermi energy. This reflects the fact that the main difference between the band structures of Snow and of Christensen with the present band structure is that our d bands, chosen to agree with the photoemission results of Eastman and Cashion,¹² are wider.

Finally, we would like to make a few brief remarks about the nature and use of the phase-shift parametrization scheme, and the possibilities for improvement in the scheme.

In this regard, we would first like to point out that rather than choosing the $\tan\eta_l$'s as the fundamental quantities to parametrize, we could have chosen to parametrize the logarithmic derivatives of the radial wave function, which in turn give the $\tan\eta_l$ by Eq. (2). We intend to investigate further the question of the relative merits of parametrizing the logarithmic derivatives as opposed to parametrizing the phase shifts directly as done in the present

work. However, we will make a few brief remarks here.

The attraction of parametrizing the logarithmic derivatives is that those quantities contain all the information about the potential, and only that information. It is possible that the avoidance of lumping in information about the Bessel functions might lead to a somewhat simpler and/or more accurate parametrization of the logarithmic derivative than of the $\tan\eta_l$ directly. (This is especially true for $l=0$, where the Bessel function gives a cusp in $\tan\eta_0$ at $\epsilon=0$. On the other hand, the ϵ dependence of the logarithmic derivatives is not so simple as to make likely a radical reduction in the number of parameters required.) Whether such a gain will exist in practice will probably depend on the sensitivity of the accuracy of the energy eigenvalues on the degree of cancellation in the numerator of Eq. (2), i. e., a small absolute error in the logarithmic derivative can imply a large relative error in $\tan\eta_l$ when $\tan\eta_l$ is small. Such cancellation reflects the similarity of the band energies to the free-electron energy; and, of course, as $\tan\eta_l$ goes to zero such effects do not matter. (Indeed, just such cancellation effects provide the justification for neglecting $\tan\eta_l$'s for $l > 2$.) The only question is a quantitative one, viz., do cancellation effects cause significant inaccuracy before $\tan\eta_l$ becomes negligible? (One should remember that because of our demand for high accuracy, we may be forced to concern ourselves with rather small differences.) An investigation we have initiated should answer such questions.

In connection with the possible utility of our study of the energy dependence of the electronic phase shifts, we should point out that there has been considerable recent interest in a related, but different use of the phase-shift parametrization concept than

that made here.^{24,25} This is the adjustment of the Fermi energy and the phase shifts at that energy to very accurately fit experimental Fermi-surface data. There is a severe problem for this technique in that it fails to provide a unique set of phase shifts and Fermi energy. Constraining the variation of the phase shifts with energy to satisfy (14), (16), and (18) may help to eliminate this ambiguity.

In conclusion, our phase-shift parametrization scheme aims at accurately describing the energy bands across a large energy range. One of its great virtues is that this scheme allows empirical adjustment of the band structure (in effect correcting the initial first-principles potential by incorporating experimental data) to be made in a particularly physically transparent way. The cost for this combination of accuracy and conceptual physical simplicity is having to deal with a determinantal equation requiring more time to solve than the simple secular determinantal equation used in some other schemes.^{1,2} That is, as discussed in Sec. I, we have devoted our efforts to the aim of effectively incorporating experimental information about the solid state into the potential, rather than to the aim of improving the speed of the band calculation *per se*. The main computational difficulty, of course, is in the proper treatment of the energy and \bar{k} -dependent structure coefficients. Any developments improving the speed of calculation of these coefficients, whether through improved computer tech-

nique or by the use of approximations, would greatly enhance the utility of the phase-shift parametrization scheme. This might involve deciding on some compromise between the complexity of form of the $\tan\eta_l(\epsilon)$ necessary for great accuracy and the simplicity desirable for facility in manipulations. Combining a fast approximation scheme for effectively calculating the structure coefficients with the phase-shift parametrization method would be most valuable in dealing with rather complex properties, such as strain and deformation effects, optical and magnetic properties. In any case, knowledge about the phase shifts associated with a particular atomic species as gained in the application of the phase-shift parametrization method (such as in our semi-empirical study of silver) will be of great importance in itself for understanding such properties. Since the phase shifts embody the structure-independent information about the solid, such knowledge would be particularly valuable for treating the electronic properties of different structural phases of a given element, of intermetallic compounds, and of solids such as alloys, thin films, and amorphous materials where one, at least partially, loses lattice translational symmetry.

ACKNOWLEDGMENT

The authors appreciate valuable discussions with Dr. F. S. Ham.

¹H. Ehrenreich and L. Hodges, in *Methods in Computational Physics, Energy Bands of Solids*, edited by B. Alder, S. Fernbach, and M. Rotenberg (Academic, New York, 1968), Vol. 8, Chap. 5.

²F. M. Mueller, *Phys. Rev.* **153**, 659 (1967).

³J. C. Phillips and R. Sandrock, in *Methods in Computational Physics, Energy Bands of Solids*, edited by B. Alder, S. Fernbach, and M. Rotenberg (Academic, New York, 1968), Vol. 8, Chap. 2.

⁴Brief summaries of our scheme have appeared in B. R. Cooper, E. L. Kreiger, and B. Segall, *Phys. Letters* **30A**, 333 (1969); in *Computational Methods in Band Theory*, edited by P. M. Marcus, J. Janak, and A. Williams (Plenum, New York, to be published). The idea of developing such a scheme had its genesis in a suggestion made by B. Segall and F. S. Ham, in *Methods in Computational Physics, Energy Bands of Solids*, edited by B. Alder, S. Fernbach, and M. Rotenberg (Academic, New York, 1968), Vol. 8, Chap. 7.

⁵For a review of the KKR method see the article by B. Segall and F. S. Ham cited in Ref. 4.

⁶B. Segall, *Phys. Rev.* **125**, 109 (1962).

⁷B. Segall, General Electric Research Laboratory Report No. 61-RL-2785G, 1961 (unpublished).

⁸We have used tabulated values of the structure coefficients calculated by B. Segall and F. S. Ham. In addition to the tabulation contained in General Electric Research Laboratory Report No. 61-RL-2876G, 1961 (unpublished), we have used extensive additional tabulations contained

in notebooks compiled by Segall.

⁹B. Segall, *Phys. Rev.* **124**, 1797 (1961).

¹⁰B. R. Cooper, H. Ehrenreich, and H. R. Philipp, *Phys. Rev.* **138**, A494 (1965).

¹¹C. N. Berglund and W. E. Spicer, *Phys. Rev.* **136**, A1044 (1964).

¹²D. E. Eastman and J. K. Cashion, *Phys. Rev. Letters* **24**, 310 (1970).

¹³D. J. Roaf, *Phil. Trans. Roy. Soc. London* **A255**, 135 (1962); D. Shoenberg, *ibid.* **A255**, 85 (1962).

¹⁴H. Ehrenreich and H. R. Philipp, *Phys. Rev.* **128**, 1622 (1962).

¹⁵H. V. Bohm and V. J. Easterling, *Phys. Rev.* **128**, 1021 (1962).

¹⁶R. W. Morse, values quoted in Ref. 15; and private communication.

¹⁷Besides the quantities discussed here, there is an additional small check on the accuracy with which our semiempirical band structure describes the experimentally determined electronic structure of silver. This is the over-all *d*-band width. This will differ slightly from the energy difference $E(L_{32}) - E(X_3)$ used in (d) of Sec. III; and in using the value 3.5 eV to characterize the *d*-band width of Eastman and Cashion, we indeed chose an energy that clearly did not extend from edge to edge of the *d*-band complex. The edge-to-edge width of the *d*-band complex is given by the energy difference $E(X_3) - E(X_1) = 3.94$ eV for our semiempirical Ag band structure. Subsequent to the completion of the present manuscript, a

paper by Smith [N. V. Smith, Phys. Rev. B **3**, 1862 (1971)] appeared giving the energy difference $E(X_2) - E(X_1)$ of 3.88 eV, obtained from a very detailed analysis of his photoemission data.

¹⁸E. C. Snow, Phys. Rev. **172**, 708 (1968).

¹⁹N. E. Christensen, Phys. Status Solidi **31**, 635 (1969).

²⁰S. Bhatnagar, Phys. Rev. **183**, 657 (1969).

²¹P. E. Lewis and P. M. Lee, Phys. Rev. **175**, 795 (1968).

²²R. L. Jacobs, J. Phys. C **1**, 1296 (1968); **1**, 1307 (1968).

²³V. Heine and I. Abarenkov, Phil. Mag. **9**, 451 (1964); I. Abarenkov and V. Heine, *ibid.* **12**, 529 (1965); A. O. E. Animalu and V. Heine, *ibid.* **12**, 1249 (1965).

²⁴M. J. G. Lee, Phys. Rev. **187**, 901 (1969).

²⁵J. F. Cooke, H. L. Davis, and R. F. Wood, Phys. Rev. Letters **25**, 28 (1970).

PHYSICAL REVIEW B

VOLUME 4, NUMBER 6

15 SEPTEMBER 1971

Radio-Frequency Size Effect in Magnesium[†]

Paul Roach

Department of Physics, University of Chicago, Chicago, Illinois 60637

(Received 2 November 1970)

The radio-frequency size effect has been used to study the Fermi surface of magnesium. These experimental data are then compared with a detailed mathematical model of the Fermi surface. The agreement is very good, confirming the accuracy of the experimental technique and the mathematical model. However, certain problems of data interpretation seriously limit the applications of the radio-frequency size effect for the study of unknown Fermi surfaces. Experiments for which this technique is better suited are discussed.

I. INTRODUCTION

The radio-frequency size effect (RFSE) is a relatively recent technique for the study of the Fermi surfaces of metals. Since the initial experiments on tin by Gantmakher,¹ this technique has been applied to an ever increasing variety of metals. The primary attraction of this method is its ability to give accurate measurements of Fermi-surface caliper dimensions. When combined with the relatively simple experimental apparatus that is required, the RFSE offers a powerful and convenient tool for the study of metallic Fermi surfaces.

Full references to the early work with the RFSE are contained in the review articles by Gantmakher² and by Walsh.³ Most of this work falls into two categories: the study of known simple Fermi surfaces in order to obtain a better understanding of the RFSE itself, and the study of unknown complex Fermi surfaces in order to learn about the band structure of the particular metal. Both of these approaches fail to define the limitations to the use of the RFSE: the former, because a simple surface, as in potassium,⁴ does not present the problems of interpretation that can arise with a complex surface; the latter, because an unknown surface, as in gallium,⁵ provides little or no basis for resolving problems of interpretation.

One of the purposes of this paper is to define more clearly some of the limitations in the usefulness of the RFSE. The results of this study make it possible to suggest areas where the RFSE

can be used to great advantage. But to do this, it is essential to use a metal whose Fermi surface is both topologically complex and well known.

Magnesium is well suited to these goals. On the one hand, it has a geometrically complex Fermi surface which can be expected to cause a variety of complicated effects in the experimental data. It is just such effects that are important for this study since their interpretation is one of the major problems in the use of the RFSE.

On the other hand, the Fermi surface has been accurately measured and described in terms of a detailed band-structure model by Stark *et al.*⁶⁻⁸ Calculations based on this mathematical model can be compared directly with the experimental data, even for the most complicated signals. In this way, the accuracy and reliability of the experimental method can be clearly defined.

II. SIZE EFFECT

From a purely experimental viewpoint, the RFSE measures the rf power absorption in a metal sample as a function of static magnetic field strength. The problem then is to relate this power absorption to the motion of the electrons in the sample. As is implied by the name "size effect," this motion is expected to be strongly influenced by the presence of the sample boundaries as well as by the static magnetic field and the Fermi-surface geometry.

The purpose of the rf field is to interact with the electrons in the metal and thereby probe their motion. But since the rf field penetrates only a